Optimized Scattering Power Spectral Density of Photovoltaic Light-Trapping Patterns

M.-Claire van Lare and Albert Polman*

Center for Nanophotonics, FOM Institute AMOLF, Science Park 104, 1098 XG Amsterdam, The Netherlands

Supporting Information

ABSTRACT: We present a generic approach for the optimization of light-trapping patterns for thin-film solar cells. The optimization is based on tailoring the spatial frequencies in the light-trapping pattern to the waveguide modes supported by the thin-film solar cell stack. We calculate the dispersion relations for waveguide modes in thin-film Si solar cells and use them to define the required spatial frequency band for light trapping. We use a Monte Carlo algorithm to optimize the scattering power spectral density (PSD) of a random array of Mie scatterers on top of a-Si:H cells. The optimized particle array has a PSD that is larger in the desired spatial frequency range than the PSD of a random array and contains contributions at more spatial frequencies than the PSD of a periodic array. Three-dimensional finite-difference time-domain simulations on thin-film solar cells with different light-trapping patterns show that the optimized particle array results in more efficient light trapping than a random array of Mie scatterers. We use the same approach to design a random texture and compare this to the Asahi-U-type texture. We show that the optimized texture outperforms the Asahi-U pattern and an optimized periodic pattern. The light-trapping patterns presented avoid the ohmic absorption losses found in metallic (plasmonic) patterns. They can be tailored to specific spatial frequency ranges, do not contain materials that are incompatible with high-temperature processes, nor require patterning of the active layer. Therefore, they are applicable to nearly all types of thin-film solar cells.

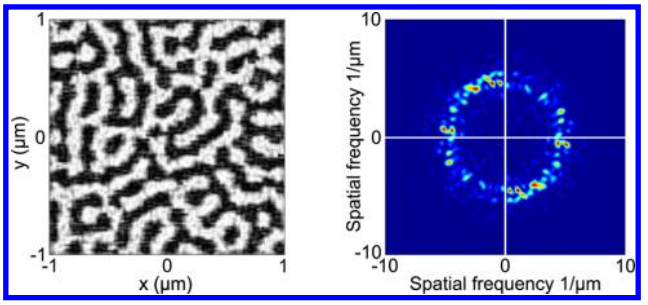

KEYWORDS: *scattering, power spectral density, thin-film solar cells, light trapping, dielectrics*

Thin-film solar cells combine the advantages of potentially lower fabrication costs with the possibility of mechanically flexible devices. However, a major problem with these thin absorber layers is the relatively poor absorption of light. To enhance light absorption in thin-film solar cells, light trapping is required, in which nanostructures are used to trap the light in the absorber layer.[1,2] Many different light-trapping geometries have been studied, including randomly textured transparent conductive oxides (TCOs) and random and periodic arrays of nanocones, nanodomes, nanorods, and nanoparticles.[3−13] Multiple papers compare random and periodic light-trapping patterns.[10,14−20] The diffractive properties of the scattering pattern depend on its power spectral density (PSD), which is the spatial Fourier transform of the scattering pattern. Periodic patterns show high peaks in PSD at the spatial frequencies that correspond to the array periodicity, but their PSD spectra consist of only very few peaks. For broadband light trapping, a broader distribution of spatial frequencies is required. Random patterns contain a broad distribution of spatial frequencies. However, for each spatial frequency the PSD is much lower than the PSD of the periodic pattern at the spatial frequency that corresponds to the array pitch. Furthermore, random patterns do not have all of their peaks in PSD in the spatial frequency range that is required for waveguide mode coupling.

Quasi-random patterns have a broader distribution of spatial frequencies than periodic patterns and have peaks with higher PSD than random patterns. However, their distribution of spatial frequencies cannot be tailored to maximize overlap with a specified set of waveguide modes. From Parseval's theorem we know it is not possible to enhance the PSD at all spatial frequencies simultaneously without increasing the volume of the scatterers,[21] but the possibility exists to enhance the PSD in the range of spatial frequencies required to couple to waveguide modes by reducing the PSD outside this region.

Other groups have demonstrated the possibility to design light-trapping patterns that contain optimized spatial frequency spectra.[6,22−24] In this paper we base the optimization of the scattering pattern on the waveguide modes supported by the thin-film geometry. We calculate the dispersion relations for the modes supported by the thin-film stack and use them to define the upper and lower boundaries for the spatial frequencies required for waveguide mode coupling. Furthermore, knowledge of the wavevector spectrum enables further tuning of the scattering spectrum to spectral ranges where light trapping is most important, i.e., where the semiconductor is least absorbing. We present the optimization of state of the art

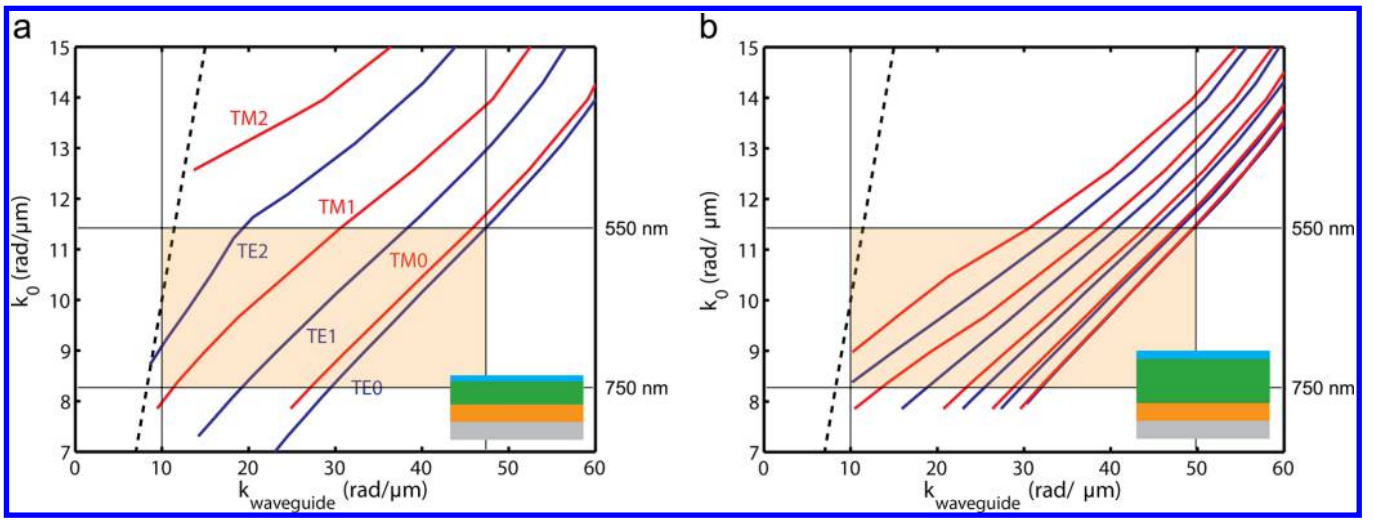

Figure 1. Dispersion relations for TE (blue) and TM (red) waveguide modes in thin-film a-Si:H solar cells with an i-layer thickness of (a) 145 nm and (b) 350 nm. Insets show the device geometry with all different layers: Ag (gray), Al-doped ZnO (AZO) (orange), a-Si:H (green), and ITO (cyan). The black horizontal lines in (a) and (b) indicate the incident spectral band for which waveguide mode coupling is required. The orange-shaded areas depict the overlap between this spectral band and the waveguide modes; the vertical black lines show the corresponding range of spatial frequencies that is required for light trapping.

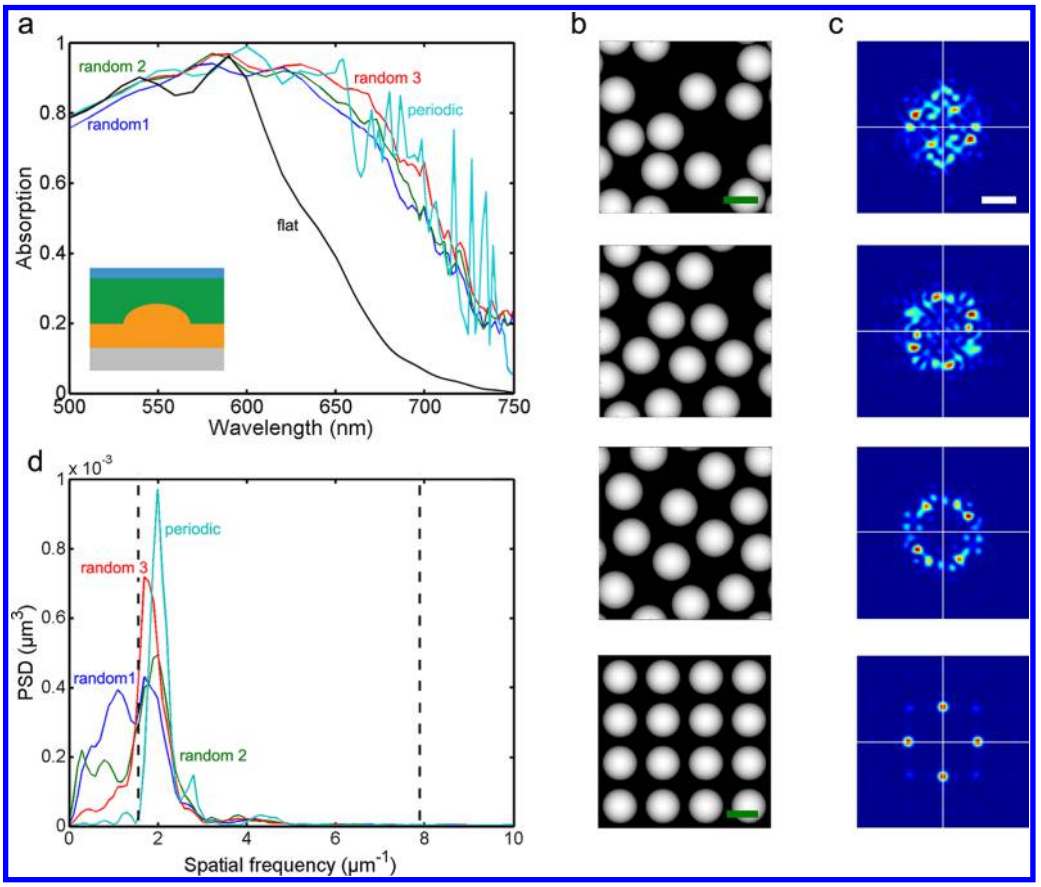

Figure 2. (a) Simulated absorption in 350 nm a-Si:H solar cells with arrays of AZO hemispheres with r = 225 nm at the a-Si:H AZO interface. Results are shown for a flat cell (black), periodically patterned cell (cyan), and randomly placed particles in a 2 × 2 μm^2 unit cell with a minimum particle spacing of 450 nm (blue), 500 nm (green), and 540 nm (red). (b) Different particle arrays used in the simulation, from top to bottom: a 2 × 2 μm^2 box with random arrays with a minimum center-to-center distance of 450, 500, and 540 nm and a 2.2 × 2.2 μm^2 box with a periodic array. The scale bar in the top figure corresponds to 400 nm and indicates the scale for the first three configurations. The scale bar in the periodic array indicates 440 nm. (c) 2D PSD spectra of particle arrays shown in (b). The scale bar indicates 2 μm^{-1}. (d) PSD(f_r) for the different geometries shown in (b). The horizontal and vertical white lines indicate the axes through the origin. Data are shown for a periodic particle array (cyan) and random particle arrays with a minimum center-to-center distance of 450 nm (blue), 500 nm (green), and 540 nm (red). The vertical dashed lines indicate the minimum and maximum spatial frequencies required for light trapping.

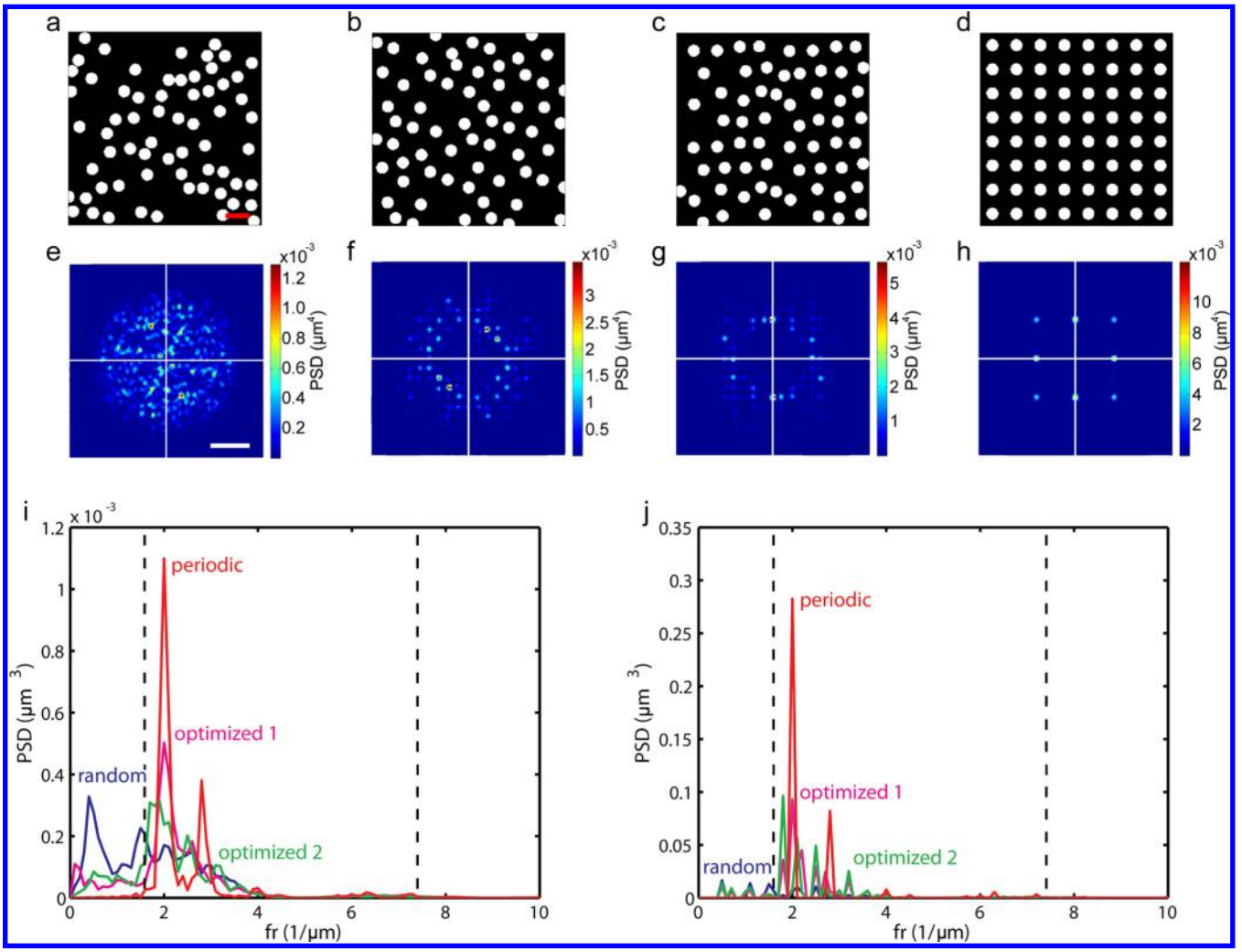

Figure 3. (a–d) Particle arrays in a 4×4 μm^2 box. Different array geometries are shown: a random array (a), two different optimized arrays (b, c), and a periodic array (d). The scale bar indicates 800 nm. (e–h) Corresponding 2D PSD spectra. The scale bar in these images corresponds to 2 μm^{-1}, and the horizontal and vertical white lines indicate the axes through the origin. PSD(f_r) is shown for (i) a single box with particles and (j) including periodic boundaries for periodic (red), random (blue) optimized 1 (magenta), and optimized 2 (green) array geometries. The vertical dashed lines in (i) and (j) indicate the minimum and maximum spatial frequencies required for light trapping.

light-trapping patterns that can be applied to nearly all thin-film solar cells. The patterns consist of either textured TCOs or arrays of dielectric resonant scatterers, which makes them compatible with all thin-film solar cell types, including those processed at high temperatures, and at the same time parasitic absorption losses in the light-trapping patterns are minimal. We present an in-depth study of these patterns in which we relate peaks in simulated absorption enhancement to spatial frequencies in the scattering patterns. The insights presented are generic and can be applied to nearly all thin-film solar cell geometries.

RESULTS

We apply the patterns to thin-film hydrogenated amorphous silicon (a-Si:H) solar cells. Because of the high refractive index of a-Si:H, light is very well confined in the waveguide layer. Figure 1 shows the dispersion relations of the waveguide modes of two cell geometries considered in this paper. The modes were calculated using a mode solving code that finds the solutions for Maxwell's equations based on the transfer matrix method.[25,26] Both geometries consist of a stack of Ag, Al-doped ZnO (AZO), a-Si:H, and indium tin oxide (ITO), schematically shown as insets in Figure 1a and b. In Figure 1a the a-Si:H layer has a thickness of 145 nm. This geometry supports only six waveguide modes in the absorber layer, three TE modes (blue) and three TM modes (red). The black dashed line shows the light line in air. All modes are located to the right of the light line, meaning that they are purely bound and cannot couple to free-space radiation. All modes have a smaller slope than the light line, indicating an effective index higher than 1. The horizontal black lines in this figure indicate the incident wavelength range for which light trapping is required, which is 550–750 nm. To achieve light trapping, this spectral band needs to be coupled to waveguide modes; this can be achieved by diffraction from a pattern that contains spatial frequencies in the range that overlaps with the wave vectors of the waveguide modes. The lower bound of the spatial frequency range that is required for light trapping is given by the light line in air. For this value we take an incident frequency of 10 rad/μm; this corresponds to a spatial frequency of 10 rad/μm, or an inverse wavelength of 1.6 μm^{-1}. The upper limit of the required spatial frequency range corresponds to the spatial frequency for which the lowest order mode still overlaps with the incident spectral band; this is a spatial frequency of 47.1 rad/μm (7.4 μm^{-1}). In

the geometry in Figure 1b the a-Si:H layer thickness is 350 nm (corresponding to the thickness of a-Si:H solar cells in our previous experimental work[13,27]). The thicker absorber layer in this geometry supports more waveguide modes than the thin layer in Figure 1a. Light trapping is required between 550 and 750 nm, which means that spatial frequencies between 10 and 49.7 rad/μm (1.6 and 7.9 μm^{-1}) are required, quite similar to the required spatial frequency range for the 145 nm thick cell.

Three-dimensional finite-difference time-domain (FDTD) simulations were used to calculate the absorption of normal-incident light in the active layer of the solar cell stack of Figure 1b (see Methods section). Figure 2 shows the result for cells with different arrays of AZO particles at the AZO/a-Si:H interface (see inset) and a flat reference cell (black). All geometries have similar particle size and density corresponding to an (average) array pitch of 550 nm. The periodic array (cyan) results in the highest absorption and has sharp peaks, which are signatures of waveguide mode coupling. The red, blue, and green lines are simulations for 2×2 μm^2 unit cells with different random particle arrays. They show a broadband enhancement rather than distinct peaks, due to the random geometry of the unit cell. The blue line shows the most random configuration (top geometry in Figure 2b). This configuration is obtained by placing particles in the unit cell at positions determined by a random number generator for x and y coordinates with the restriction that overlap is not allowed. To obtain the other configurations, a local search algorithm is used to find a configuration in which all particles have a minimum center-to-center distance of 500 nm (second geometry in Figure 2b) or 540 nm (third geometry in Figure 2b) (see Methods section). Compared to the random geometry, the absorption in the a-Si:H layer, shown in Figure 2a, is enhanced for the more ordered geometry with a 500 nm center-to-center distance (green) and further enhanced for the geometry with the 540 nm center-to-center distance (red). This trend is reproducible for different random initializations and unit cell sizes (not shown).

Figure 2c shows the PSD of the four different patterns, defined by

$$\mathrm{PSD}(f_x, f_y) \equiv \frac{1}{L^2}\left|\sum_n \sum_m h_{mn} e^{-2\pi i \Delta L (f_x n + f_y m)} \Delta L^2\right|^2 \quad (1)$$

where f_x and f_y are the spatial frequencies in the x and y direction, respectively, L is the length of the pattern, h_{mn} is the height at position m, n, and ΔL is the pixel size in the height map.[28] The most random pattern shows a filled circle with a broad distribution of spatial frequencies. A large fraction of the total PSD is at spatial frequencies that are to the left of the light line and thus not useful for mode coupling. Increasing the order by increasing the minimum distance results in a reduction of PSD at low frequencies; the PSD changes from a circle into a ring. The periodic pattern shows distinct peaks at spatial frequencies corresponding to the inverse array pitch. Figure 2d shows $\mathrm{PSD}(f_r)$, with $f_r^2 = f_x^2 + f_y^2$, for the different patterns. The periodic pattern shows a sharp peak at 1.8 μm^{-1}, corresponding to the (0,1) diffraction order in the array, and a second peak at 2.6 μm^{-1}, corresponding to the (1,1) diffraction order. Higher order peaks are observed at larger spatial frequencies at very small intensity. The intensity of these peaks is low because the form factor, which is the spatial Fourier transform of the particle shape,[29] has low intensity at these frequencies. The finite width of the peaks is due to the finite size of the pattern. The peaks would be δ-functions in the case of an infinite array size. Compared to the random patterns, the periodic pattern has an overall higher PSD at frequencies above 1.6 μm^{-1}. This leads to more efficient mode coupling and, hence, overall higher simulated absorption spectrum. Increasing the order in the random pattern (blue to green to red) results in a higher PSD above 1.6 μm^{-1}, which is in the range useful for mode coupling. This is in agreement with the trend in simulated absorption that also shows increasing absorption in the red spectral range with increasing order of the light-trapping pattern.

To have more control over the PSD of the scattering pattern and match it better to the desired spatial frequency pattern, we optimize a random scattering pattern using a Monte Carlo algorithm (see Methods section). Figure 3 shows a random (a), two different optimized, referred to as optimized 1 and optimized 2 (b, c), and a periodic array geometry (d) with their corresponding 2D PSD spectra (e–h). The two different optimized configurations are generated using different random initializations. Since the particles are smaller than in the array geometry in Figure 2, they can have smaller center-to-center distances without overlapping, which means that also larger spatial frequencies can be present. Therefore, the PSD of the random array (e) shows a broader distribution of spatial frequencies than the PSD of the random array in Figure 2c. The optimized array geometries show more order than the random geometry, which is also visible in the corresponding PSD spectra. The PSD at frequencies around zero is significantly reduced, and the PSD at frequencies above the light line is enhanced. The response of the random and optimized random patterns is not isotropic, and a few high peaks are observed. The random pattern will give an isotropic response in the case of an infinitely large box. Figure S1 in the Supporting Information section shows that the PSD of a random particle array generated in the same way becomes isotropic when increasing the box size. Regarding the nonisotropic resonse of the optimized patterns, there is no preferred directionality in the optimization algorithm; particles are moved in all directions with equal probabilities.

At frequencies above 4 μm^{-1}, no substantial enhancement in PSD is observed after the optimization. This is due to the restriction that the particles are not allowed to overlap. Figure 3d shows the periodic geometry, which has similar particle size and density to the geometries in Figure 3a–c. The PSD of the periodic pattern (Figure 3h) shows higher peaks than the PSD of the optimized random array geometries. Figure 3i shows the $\mathrm{PSD}(f_r)$ for the four different array geometries. The vertical dashed lines indicate the range of spatial frequencies that overlaps with the waveguide modes in the 550–750 nm incident spectral range. The difference in PSD at frequencies below the light line (1.6 μm^{-1}) for the different patterns is clearly visible. The random pattern (blue) has a large fraction of its PSD at frequencies that are too low for coupling to bound waveguide modes. The PSD of the optimized patterns (green, magenta) is significantly reduced at these frequencies, but it is still larger than zero. The periodic pattern (red) shows PSD only at frequencies above the light line, and the peaks at 2.0 and 2.8 μm^{-1} are much larger than the peaks in the PSD of the optimized pattern. In contrast, the PSD of the optimized patterns contains a broad distribution of spatial frequencies above the light line.

The unit cells we optimized have a size of 4×4 μm^2. In order to use them as a light-trapping geometry in an FDTD

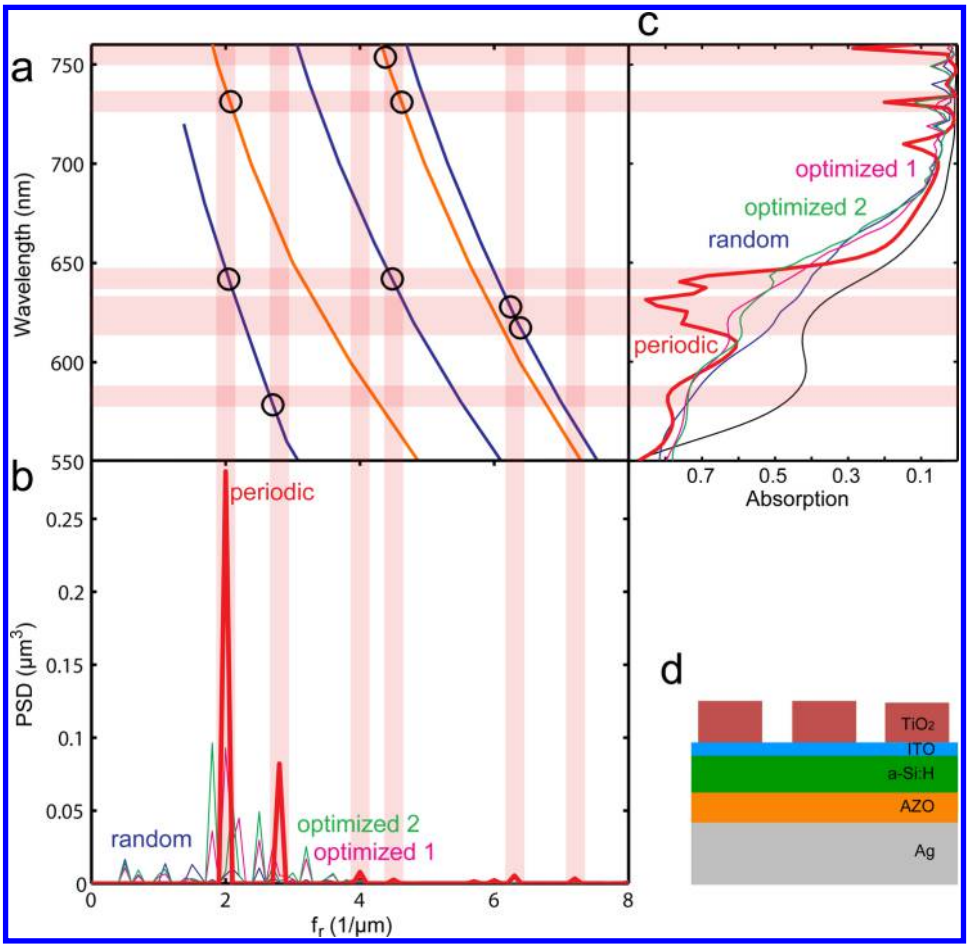

Figure 4. (a) Dispersion relations for TE (blue) and TM (red) waveguide modes in a 145 nm a-Si:H cell. (b) PSD(f_r) for periodic (red), random (blue), and optimized (green, magenta) array geometries. (c) Simulated absorption in thin-film a-Si:H cells with different scattering patterns. Data are shown for cells with periodic (red), random (blue), and optimized (green, magenta) array geometries. (d) Schematic cross section of the cell geometry, consisting of Ag (gray), AZO (orange), a-Si:H (green), ITO (cyan), and TiO_2 (brown). This figure shows the relation between the PSD spectrum and light trapping for the periodic pattern. The semitransparent red vertical lines in (a) and (b) relate the peaks in the PSD of the periodic pattern to the waveguide modes and show at which incident wavelengths mode coupling is possible. These incident wavelengths are indicated by the horizontal semitransparent red lines. Black circles in (a) indicate intersections between peaks in PSD and waveguide modes at wavelengths for which peaks in simulated absorption are observed.

simulation, for all four light-trapping patterns the unit cells were combined with periodic boundary conditions. This was done by replicating the box in the x and y direction. This also influences the PSD of the light-trapping patterns. The PSD of the patterns in combination with periodic boundary conditions (for 25 replications of the unit cell) is shown in Figure 3j. The periodic boundaries lead to changed PSD spectra compared to the spectra for a single unit cell in Figure 3i. The periodic pattern (red) shows narrower peaks than in 3i; increasing the box size to infinity would lead to δ-functions at the spatial frequencies corresponding to the array pitch. The random and optimized random patterns (blue, green, magenta) show multiple narrow peaks due to the random unit cell in combination with periodic boundaries. Comparing the PSD for the different patterns shows similar trends to those in Figure 3i. The random (blue) pattern has a low PSD in the frequency range of interest. The PSD is substantially larger for the optimized patterns (green, magenta) and even larger for the periodic pattern. At spatial frequencies between 3.0 and 3.9 μm^{-1} all random patterns have a larger PSD than the periodic pattern.

To demonstrate the influence of the PSD of the scattering pattern on the absorption enhancement of the solar cell, Figure 4 shows the dispersion relations of the waveguide modes in the thin-film stack (a), together with the power spectral density of the scattering patterns (b), and the simulated absorption in the a-Si:H layer (c) of the solar cell geometry shown in (d). The cell geometry consists of 200 nm of Ag (gray), 130 nm of AZO (orange), 145 nm of a-Si:H (green), 80 nm of ITO and an array of TiO_2 particles (brown) with a radius of 125 nm, a height of 200 nm, and an (average) pitch of 500 nm. Figure 4 depicts this relation between PSD and light trapping for the periodic scattering pattern (red). The red semitransparent vertical lines through the PSD spectrum and the dispersion relations of the modes connect the spatial frequencies in the PSD spectrum of the periodic pattern to the waveguide modes. Intersections between these lines and waveguide modes present incident wavelengths at which mode coupling is possible for the periodically patterned cell, indicated by horizontal red semi-transparent lines. Intersections between waveguide modes and peaks in the PSD spectrum that result in peaks in the simulated absorption spectrum are marked with black circles. The absorption enhancement for the periodically patterned cell shows a broad peak between 610 and 650 nm. The reason that this peak is so broad is twofold. First, in this incident spectral

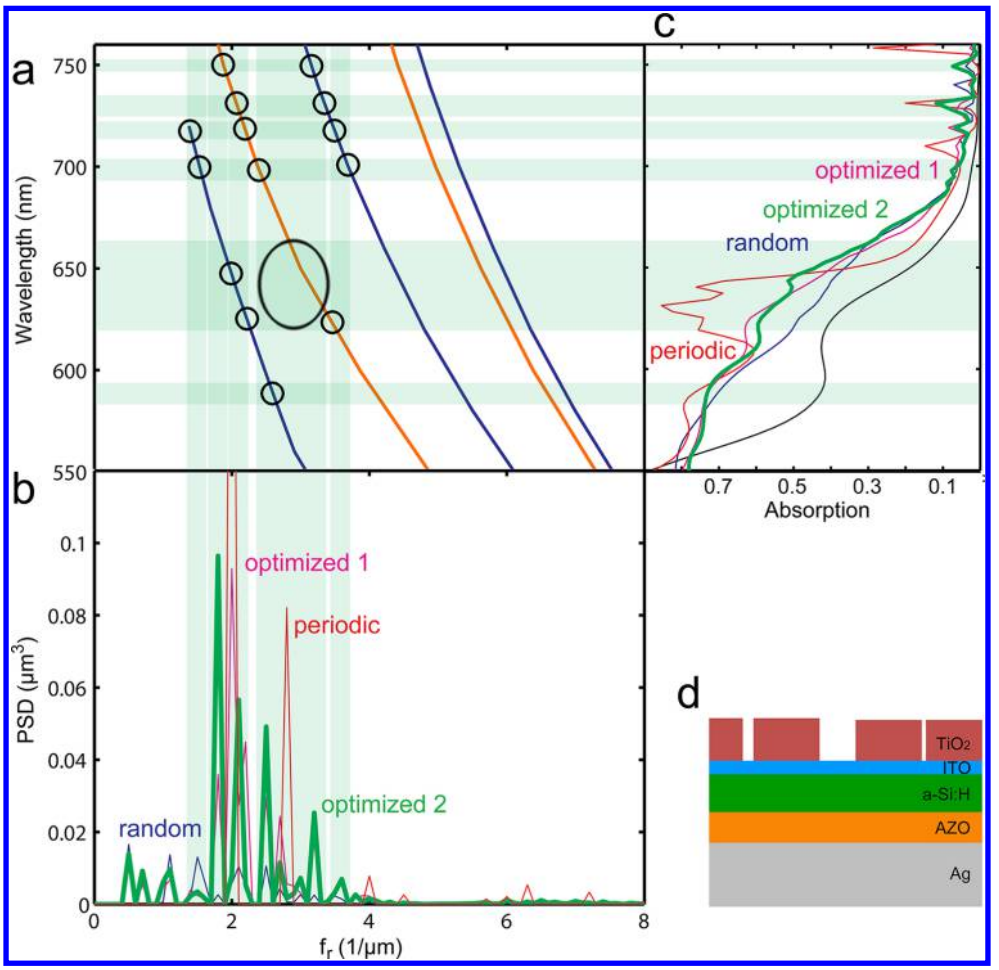

Figure 5. (a) Dispersion relations for TE (blue) and TM (red) waveguide modes in a 145 nm a-Si:H cell. (b) PSD(f_r) for optimized 2 (green), periodic (red), random (blue), and optimized 1 (magenta) array geometries. (c) Simulated absorption in thin-film a-Si:H cells with different scattering patterns. Data are shown for cells with periodic (red), random (blue), and optimized (green, magenta) array geometries. (d) Schematic cross section of the cell geometry, consisting of Ag (gray), AZO (orange), a-Si:H (green), ITO (cyan), and TiO_2 (brown). This figure shows the relation between the PSD spectrum and light trapping for one of the optimized random patterns. The semitransparent green vertical lines in (a) and (b) relate the peaks in the PSD of the optimized random pattern to the waveguide modes and show at which incident wavelengths mode coupling is possible. These incident wavelengths are indicated by the horizontal semitransparent green lines. Black circles in (a) indicate intersections between peaks in the PSD and waveguide modes at wavelengths for which peaks in simulated absorption are observed.

band there are multiple crossings between the PSD and waveguide modes. The highest peaks in the PSD spectrum at 2 μm^{-1} intersect with the TE_2 mode, the peak at 4.5 μm^{-1} intersects with the TE_1 mode, and the peak at 6.4 μm^{-1} intersects with the TE_0 and the TM_0 modes. Second, in this spectral range absorption in the a-Si:H layer is still quite strong, which causes an uncertainty in the wavevector of the waveguide modes. Another broad peak is observed in the simulated absorption at 585 nm. This peak is attributed to coupling to the TE_2 mode by the peak in the PSD spectrum at 2.8 μm^{-1}.

At wavelengths of 730 and 760 nm, two distinct peaks are observed in the simulated absorption spectrum. At these wavelengths, the absorption in the a-Si:H layer is very weak, which leads to more well-defined wavevectors of the waveguide modes than at lower wavelengths and, hence, to narrower peaks in the absorption spectrum. The peaks at 730 and 760 nm correspond to coupling to the TE_1 and the TM_0 mode, respectively. The small peak at 710 nm cannot be related to mode coupling, and it was found that this peak depends on the particle radius. At wavelengths below 550 nm the absorption in the a-Si:H layer is enhanced by an antireflection effect caused by preferential forward scattering by the Mie scatterers (not shown).[30]

Similar to the light trapping shown in Figure 4 for the periodic scattering pattern, Figure 5 shows the waveguide-mode coupling for the optimized random pattern "optimized 2" (green), which is the optimized pattern shown in Figure 3c. The PSD spectrum of this optimized pattern shows a broad distribution of spatial frequencies compared to the periodic pattern. All peaks in the PSD spectrum are substantially lower than the peak at 2 μm^{-1} in the PSD spectrum of the periodic pattern, which leads to the absence of very distinct peaks in the simulated absorption spectrum (Figure 5c). Many intersections between relatively small peaks in the PSD spectrum and waveguide modes are observed. The contribution of all of these intersections leads to a broadband enhancement in the simulated absorption. At wavelengths between 620 and 665 nm the simulated absorption in the cell with the optimized pattern exceeds the absorption in the cell with the periodic pattern, which is due to the multiple peaks in PSD between 2.4 and 3.3 μm^{-1}. The availability of multiple Fourier components in combinations with the strong absorption in this spectral

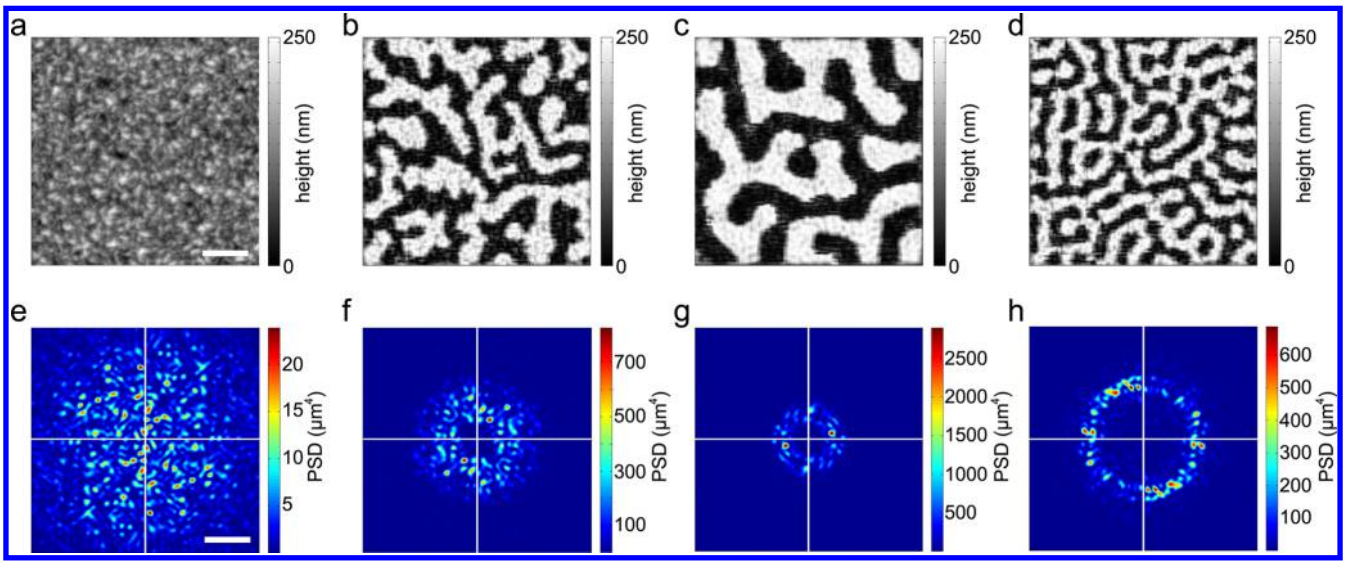

Figure 6. (a–d) Height maps for different textures with a maximum height of 250 nm. The scale bar indicates 400 nm. (a) Asahi-U-type textures optimized for PSD enhancement at spatial frequencies of (b) 1.6–7.9 μm^{-1}, (c) 1.6–4.4 μm^{-1}, and (d) 4.4–7.9 μm^{-1}. (e–h) 2D PSD spectra corresponding to textures in (a)–(d). The scale bar indicates 4 μm^{-1}, and the horizontal and vertical white lines indicate the axes through the origin.

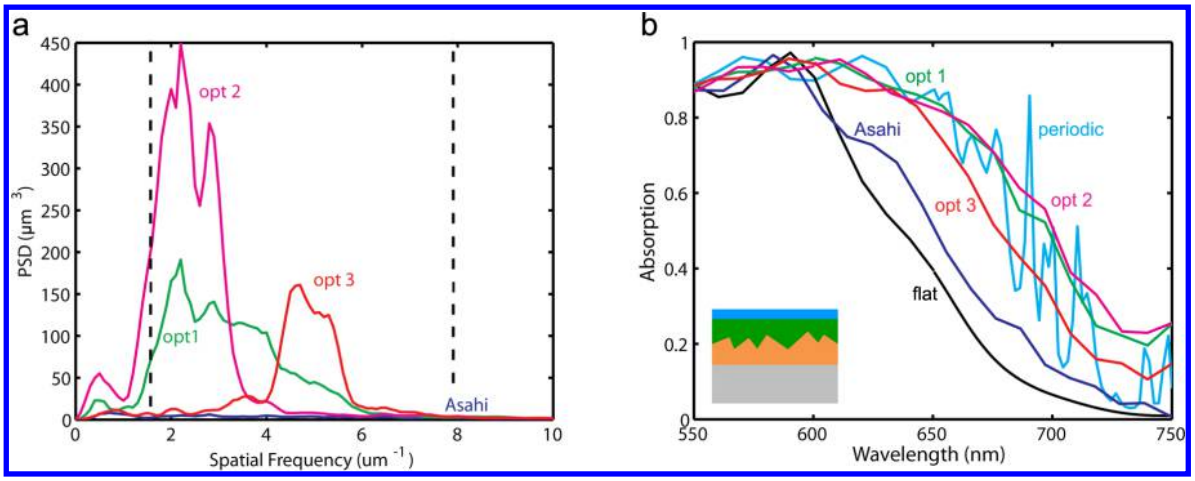

Figure 7. (a) PSD(f_r) for the different textures shown in Figure 6. Data are shown for Asahi (blue), opt 1, optimized for spatial frequencies 1.6–7.6 μm^{-1}, (green), opt 2, optimized for 1.6–4.4 μm^{-1}, (magenta), and opt 3, optimized for 4.4–7.6 μm^{-1} (red). The vertical dashed lines indicate the minimum and maximum spatial frequencies required for light trapping. (b) Simulated absorption in the a-Si:H layer of 350 nm a-Si:H cells with different textures at the a-Si:H/AZO interface. Data are shown for flat (black) and periodically patterned (cyan) cells and cells with textures Asahi-U type (blue), opt 1 (green), opt 2 (magenta), and opt 3 (red). The inset shows a schematic cross section of the device geometry, consisting of Ag (gray), AZO (orange), a-Si:H (green), and ITO (cyan).

range causes broadband light trapping. The simulated absorption for the optimized geometry also contains the broad peak between 610 and 650 nm that is observed for the periodic pattern. However, the absorption is lower in this spectral range for the optimized pattern. We attribute this to the lack of the large peak at 2 μm^{-1} that is present in the PSD of the periodic pattern. Overall the optimized pattern results in lower simulated absorption than the periodic pattern, but it performs significantly better than the random pattern (blue). The improvement with respect to the random pattern is consistent with the increased PSD spectrum after the optimization. The other optimized pattern, optimized 1, results in a somewhat different absorption spectrum than optimized 2, but also performs significantly better than the random pattern. Figures 4 and 5 do not show a one-to-one relationship between the intensity of the peaks in the PSD spectrum and the peaks in the absorption spectrum. The PSD spectrum is a first prerequisite for efficient scattering, and optimizing the PSD spectrum leads to enhanced coupling to the waveguide modes. However, for a fully quantitative model, the mode-coupling strength, which depends on the overlap between the waveguide modes and the scattered field, is required. Evaluation of the coupling strength goes beyond the scope of this paper.

OPTIMIZATION OF RANDOM TEXTURES

Due to the size, shape, and nonoverlap restrictions of the array of Mie scatterers, there is limited flexibility in the PSD spectra that can be obtained by optimization. This limitation is particularly found when trying to enhance the PSD at larger spatial frequencies, which overlap with the lower order waveguide modes. In order to design a scattering pattern with a more tunable PSD, we optimize a random texture (see Methods section). Figure 6 summarizes the results of the random texture optimization. Figure 6a shows the height map

of the Asahi-U-type pattern and its corresponding 2D PSD spectrum. This pattern contains a very broad range of spatial frequencies, and many of them are too low or too high in order to be useful for mode coupling in the cell geometries discussed in this work. Figure 6b shows the height map and PSD for a texture that is optimized in the spatial frequency range required to couple to the waveguide modes, which is between 1.6 and 7.9 μm^{-1}. The overall feature size is larger than in the Asahi texture, and the 2D PSD shows a more ordered geometry, in which the PSD in the useful spatial frequency range is strongly enhanced with respect to the PSD outside this range. To demonstrate that this concept can easily be applied to tailor a pattern to a specific frequency range, Figure 6c shows the optimization for a frequency range between 1.6 and 4.4 μm^{-1}, which results in an overall larger feature size than in Figure 6a and b and a large PSD in this low-frequency ring, which overlaps with the higher order waveguide modes supported by the thin-film stack. Similarly, the geometry in Figure 6d is optimized for the spatial frequency range 4.4 to 7.4 μm^{-1}, which mostly overlaps with the TM_0 and the TE_0 modes in Figure 1a. This texture contains smaller features than the texture in Figure 6a, and the PSD spectrum shows a ring in the desired frequency range.

Figure 7 shows the PSD(f_r) for the different light-trapping textures. All optimized patterns (green, red, magenta) show significantly higher PSD in this spatial frequency range than the Asahi pattern (blue). Comparing the PSD of the optimized pattern clearly demonstrates how well a pattern can be optimized to only have elevated PSD in a certain spatial frequency range. Of the optimized patterns, opt 2 has the largest PSD integrated over the spatial frequency range from 1.6 to 7.9 μm^{-1}. Figure 7b depicts the simulated absorption in the solar cell type described in Figure 1b, with patterned AZO layers, using the different textures shown in Figure 6, compared to a flat solar cell (black line). Also in these geometries, in which the absorber layer is not flat, the waveguide modes are well defined and can be calculated assuming a flat layer stack, as demonstrated in previous work.[31] The a-Si:H front interface is assumed to be flat, based on experimental data for this layer thickness, which shows no substantial front-side texture and no antireflection effect caused by the rear-side light-trapping patterns.[27] The absorption for the flat cell (black) decays rapidly in the wavelength range shown. The Asahi pattern (blue) results in enhanced absorption with respect to the flat cell, but the different optimized random patterns (magenta, green, red) perform substantially better. Of these patterns opt 2 (magenta), which is optimized for spatial frequencies between 1.6 and 4.4 μm^{-1}, shows the largest absorption enhancement, consistent with its large PSD in the spatial frequency range that overlaps with the waveguide modes. Also an optimized periodic pattern, consisting of AZO hemispheres, is shown (see Methods section). Light trapping with the patterns opt 1 and opt 2 is even larger than for the optimized periodic pattern (cyan). The pattern that is optimized to have a large PSD at frequencies of 4.4–7.9 μm^{-1} results in somewhat lower light trapping than the other two optimized patterns. This pattern also shows a lower integrated PSD in the desired frequency range. The simulations clearly demonstrate the advantage of a pattern with optimized spatial frequencies with respect to a random pattern. The random pattern has a broad distribution of spatial frequencies and also contains many components that are outside the range that is useful for light trapping. The optimized patterns are designed to contain spatial frequencies in the range that overlaps with the waveguide mode and lead to much more efficient light trapping.

Whereas in the optimization of the particle array the particles were moved, which resulted in a constant volume of scatterers, in the case of the texture optimization the volume of scatterers is not conserved. Therefore, also the total PSD is not conserved in the optimization. Compared to the Asahi-U-type pattern, the optimized textures have a substantially larger PSD is this spatial frequency range. This is due to increased contrast in the height profile. For the Asahi-U-type pattern (Figure 6a) most points in the height map are close to the mean value, while the optimized textures (Figure 6b–d) have many points in their height profile that are close to 0 or to the maximum height. Table 1 shows the RMS roughness for the different textures. The Asahi-U-type texture has a RMS roughness of 35 nm, and all three optimized textures show a substantially higher RMS roughness. Also, the different optimized scattering patterns show different RMS roughnesses. Opt 2, which is optimized for spatial frequencies of 1.6–4.4 μm^{-1}, has the highest RMS roughness, indicating the most contrast. This pattern also has the highest PSD (Figure 7a) and results in the most efficient light trapping (Figure 7b) of the three patterns.

Table 1. Light-Trapping Textures Shown in Figure 6a–d with Corresponding RMS Roughnesses

texture	RMS roughness (nm)
Asahi-U	35
opt 1	98
opt 2	103
opt 3	93

LIGHT-TRAPPING PATTERNS AND TRANSVERSE COHERENCE LENGTH OF SUNLIGHT

The sun is a partially coherent source of light. For the design of light-trapping patterns it is important to take into account the transverse coherence length of sunlight. When looking at a cross section of a beam of light, the transverse coherence length is defined as the length over which the phase is correlated; light scattered from two points that are spaced by this distance will exhibit interference.[32] If the separation between two scatterers exceeds the transverse coherence length, they will scatter independently. We showed that whereas the antireflection effect due to surface nanostructures in the blue spectral range mostly depends on the properties of single scatterers, the light trapping is determined by the spatial frequencies in the scattering pattern. The light-trapping patterns we designed show optimized spatial frequency spectra for box sizes of only 2 to 4 μm. For direct sunlight the transverse coherence length is on the order of 100 μm;[33] it is determined by the ratio of the square of the wavelength of the light to the solid angle that the sun subtends on Earth. This value of the coherence length for sunlight is far beyond the size of our light-trapping patterns, so that the analysis described in this paper is applicable. For indirect sunlight, the transverse coherence length is decreased, and further work is required to study this in more detail.[34,35]

CONCLUSION

We demonstrated a generic approach to optimize light-trapping patterns for thin-film solar cells, based on tailoring the PSD of the patterns to the waveguide modes in a specific thin-film solar cell stack. We calculated the dispersion relations for waveguide

modes in two different light-trapping geometries and use them to define the required spatial frequency range for light trapping. Using a Monte Carlo algorithm, we optimized random arrays of Mie scatterers in order to have increased PSD in this spatial frequency range while maintaining particle size and density. The optimized patterns show an elevated PSD in the spatial-frequency range of interest with respect to a random pattern and also result in more light trapping. However, an optimized periodic light-trapping pattern still outperforms this optimized random particle array. In order to have more flexibility in the optimization of light-trapping patterns, we optimize a random texture composed of smaller-size scatterers. We show that these optimized textures do have the ability to outperform optimized periodic particle arrays. We demonstrate the robustness of this approach by showing that the optimization can be used to specifically enhance the PSD in different ranges of spatial frequencies. Because of this, and since the light-trapping pattern does not require patterning of the active layer, nor contains materials that are incompatible with high-temperature processes, this concept is applicable to nearly all types of thin-film solar cells.

METHODS

FDTD Simulations. Three-dimensional FDTD simulations were done to calculate the absorption in the a-Si:H layer for different light-trapping geometries. A 5 nm mesh was used over the entire simulation volume. Perfectly matched layers (PMLs) were used at the top and bottom of the simulation volume, and periodic boundary conditions were used in the x and y direction. In the simulations on the TiO_2 cylinders at the front, particles at boundaries were repeated in neighboring boxes, to avoid the presence of incomplete particles. A plane wave was used to illuminate the geometries at normal incidence. Simulations were done for TM and TE polarization; the results shown in Figures 4, 5, and 7 were averaged over both polarizations. The results in Figure 2 are for TM polarized light. Refractive index monitors and field monitors were used to determine the absorption per unit volume in the a-Si:H layer using the relation $P_{abs} = 0.5\omega\epsilon''|E|^2$, with ω the frequency, ϵ'' the imaginary part of the permittivity, and E the electric field.

Optimization of Periodic Pattern. Three-dimensional FDTD simulations were used for the optimization of the periodic particle array. A unit cell with one hemiellipsoidal particle at the AZO/a-Si:H interface was simulated, and the parameter to optimize was the AM1.5-averaged absorption in the a-Si:H layer. The particle radius and height were varied from 125 to 300 nm, in steps of 25 nm, and the array pitch was varied from 400 to 700 nm in steps of 50 nm. All combinations of these parameters that did not result in overlapping particles were explored.

Local Search for Minimum Particle Spacing. A local search algorithm is used to generate the different random configurations in Figure 2b, in which the particles have a minimum center-to-center distance that exceeds the diameter. A particle is selected randomly using a random number generator. The particle is then moved with a randomly chosen step size and angle. The function that is then minimized is $\sum_i \sum_{j<i} \max(0, 2r + \mathrm{ms} - r_{i,j})$, with r the particle radius, ms the desired minimum spacing between two particles, and $r_{i,j}$ the distance between particle i and j.

Monte Carlo Optimization of Particle Array. The initial configuration consists of a random or periodic array of cylinders with a radius of 125 nm, height of 200 nm, and average pitch of 500 nm. This radius, height, and pitch correspond to an optimized periodic geometry. In each optimization cycle a particle is randomly selected and subsequently moved with a randomly chosen distance and angle. A widely varying step size between 1 and 700 nm is chosen in order to explore a large number of configurations. A random number generator with a long period is used to avoid ending up in local maxima too easily.[36] If a particle move results in an enhanced PSD integrated over the spatial frequency range of interest, it is accepted; otherwise it is rejected. The particle size and density are kept constant during the optimization. Different relatively small unit cell sizes of 2×2 μm^2 and 4×4 μm^2 are explored in combination with periodic boundary conditions. This gives a periodic pattern with a large unit cell that enables us to engineer the spatial frequency distribution. These unit cell sizes are chosen in order to have configurations that can be tested with three-dimensional FDTD simulations. We find that 4×4 μm^2 unit cells result in larger differences after optimization due to the larger number of degrees of freedom.

Random Texture Optimization. The starting configuration is a 2×2 μm^2 AFM scan (512×512 pixels) of the Asahi-U type pattern, the commercial light-trapping standard for thin-film Si solar cells. We use a Monte Carlo algorithm to find a configuration with the same maximum height, but an enhanced PSD in the spatial frequency range between 1.6 and 7.9 μm^{-1}. The optimization algorithm randomly selects a rectangle in the height map with a size between 15 and 30 pixels. Subsequently a height step, Δh, between -50 and 50 nm, is chosen randomly. Each pixel in the selected rectangle, except for the outer five rows ("edge pixels"), has a probability of 80% to be changed with this height step and thus a probability of 20% to not be changed. As a result, a certain pattern in the selected rectangle will be shifted by the height step. The edge pixels in the rectangle and all pixels adjacent to height-shifted pixels will be shifted by $0.5\Delta h$ in order to make a pattern with smooth transitions in height. If the height change of the randomly chosen shape results in a PSD increase and if the new pattern does not exceed the maximum height, the new configuration is accepted; otherwise it is rejected.

ASSOCIATED CONTENT

Supporting Information

The Supporting Information is available free of charge on the ACS Publications website at DOI: 10.1021/ph500449v.

AUTHOR INFORMATION

Corresponding Author

*E-mail: polman@amolf.nl.

Notes

The authors declare no competing financial interest.

ACKNOWLEDGMENTS

This work is part of the research program of FOM, which is financially supported by NWO. It is also funded by the European Research Council and NanoNextNL, a technology program of the Dutch Ministry of Economy Affairs. SARA Computing and Networking Services is acknowledged for support in using the Lisa Compute Cluster.

REFERENCES

(1) Green, M. A. Lambertian light trapping in textured solar cells and light-emitting diodes: analytical solutions. *Prog. Photovoltaics* **2002**, *10*, 235−241.

(2) Yablonovitch, E.; Cody, G. D. Intensity enhancement in textured optial sheets for solar cells. *IEEE Trans. Electron Devices* **1982**, *29*, 300−305.

(3) Basch, A.; Beck, F. J.; Soderstrom, T.; Varlamov, S.; Catchpole, K. R. Combined plasmonic and dielectric rear reflectors for enhanced photocurrent in solar cells. *Appl. Phys. Lett.* **2012**, *100*, 243903.

(4) Zhu, J.; Hsu, C.-M.; Yu, Z.; Fan, S.; Cui, Y. Nanodome solar cells with efficient light management and self-cleaning. *Nano Lett.* **2010**, *10*, 1979−1984.

(5) Battaglia, C.; Escarr, J.; Sderstrm, K.; Charrire, M.; Despeisse, M.; Haug, F. J.; Baliff, C. Nanomoulding of transparent zinc oxide electrodes for efficient light trapping in solar cells. *Nat. Photonics* **2011**, *5*, 535−538.

(6) Pala, R. A.; Liu, J. S. Q.; Barnard, E. S.; Askarov, D.; Garnett, E. C.; Fan, S.; Brongersma, M. L. Optimization of non-periodic plasmonic light-trapping layers for thin-film solar cells. *Nat. Commun.* **2013**, *4*, 2095.

(7) Soldera, M., Estrada, E., Taretto, K. Geometric light trapping in 2D and 3D structured small molecule organic solar cells. *MRS Fall Meeting*, 2012.

(8) Yu, K. J.; Gao, L.; Park, J. S.; Lee, Y. R.; Corcoran, C. J.; Nuzzo, R. G.; Chanda, D.; Rogers, J. A. Light trapping: light trapping in ultrathin monocrystalline silicon solar cells. *Adv. Energy Mater.* **2013**, *3*, 1401−1406.

(9) Battaglia, C.; Sderstrm, K.; Escarr, J.; Haug, F.-J.; Domine, D.; Cuony, P.; Boccard, M.; Bugnon, G.; Denizot, C.; Despeisse, M.; Feltrin, A.; Ballif, C. Efficient light management scheme for thin film silicon solar cells via transparent random nanostructures fabricated by nanoimprinting. *Appl. Phys. Lett.* **2010**, *96*, 213504.

(10) Isabella, O.; Campa, A.; Heijna, M. C. R.; Soppe, W.; Erven, R. V.; Franken, R. H.; Borg, H.; Zeman, M. Diffraction gratings for light trapping in thin-film silicon solar cells. *Proceedings of the 23rd European Photovoltaic Solar Energy Conference*; Valencia, Spain, 2008; pp 2320−2324.

(11) Tan, H.; Santbergen, R.; Smets, A. H. M.; Zeman, M. Plasmonic light trapping in thin-film silicon solar cells with improved self-assembled silver nanoparticles. *Nano Lett.* **2012**, *8*, 4070−4076.

(12) Rockstuhl, C.; Fahr, S.; Bittkau, K.; Beckers, T.; Carius, R.; Haug, F.-J.; Sderstrm, T.; Ballif, C.; Lederer, F. Comparison and optimization of randomly textured surfaces in thin-film solar cells. *Opt. Express* **2010**, *18*, A335−A342.

(13) van Lare, M.; Lenzmann, F.; Verschuuren, M. A.; Polman, A. Mode-coupling by plasmonic surface scatterers in thin-film Si solar cells. *Appl. Phys. Lett.* **2012**, *101*, 221110.

(14) Battaglia, C.; Hsu, C. M.; Sderstrm, K.; Escarr, J.; Haug, F. J.; Charrire, M.; Boccard, M.; Despeisse, M.; Alexander, D. T. L.; Cantoni, M.; Cui, Y.; Ballif, C. Light trapping in solar cells: Can periodic beat random? *ACS Nano* **2012**, *6* (3), 2790−2797.

(15) Kowalczewski, P.; Liscidini, M.; Andreani, L. Light trapping in thin-film solar cells with randomly rough and hybrid textures. *Opt. Express* **2013**, *21*, A808−A820.

(16) Bhattacharya, J.; Chakravarty, N.; Pattnaik, S.; Slafer, W. D.; Biswas, R.; Dalal, V. L. A Photonic-Plasmonic Structure for Enhancing Light Absorption in Thin Film Solar Cells. *Appl. Phys. Lett.* **2011**, *99*, 131114.

(17) Pattnaik, S.; Chakravarty, N.; Biswas, R.; Dalal, V.; Slafer, D. Nano-photonic and nano-plasmonic enhancements in thin film silicon solar cells. *Sol. Energy Mater. Sol. Cells* **2014**, *129*, 115−123.

(18) Sderstrm, T.; Haug, F.-J.; Niquille, X.; Ballif, C. TCOs for nip thin film silicon solar cells. *Progr. Photovolt: Res. Appl.* **2009**, *17*, 165−176.

(19) Ferry, V. E.; Verschuuren, M. A.; Lare, M. V.; Schropp, R. E. I.; Atwater, H. A.; Polman, A. Optimized spatial correlations for broadband light trapping nanopatterns in high efficiency ultrathin film a-Si:H solar cells. *Nano Lett.* **2011**, *11*, 4239−4245.

(20) Sai, H.; Fujiwara, H.; Kondo, M.; Kanamori, Y. Enhancement of light trapping in thin-film hydrogenated microcrystalline Si solar cells using back reflectors with self-ordered dimple pattern. *Appl. Phys. Lett.* **2008**, *93*, 143501.

(21) Kreyszig, E. *Advanced Engineering Mathematics*; Peter Janzow, 1999.

(22) Martins, E. R.; Li, J.; Liu, Y.; Depauw, V.; Chen, Z.; Zhou, J.; Krauss, T. F. Deterministic quasi-random nanostructures for photon control. *Nat. Commun.* **2013**, *4*, 2665.

(23) Martins, E. R.; Li, J.; Liu, Y.; Zhou, J.; Krauss, T. F. Engineering gratings for light trapping in photovoltaics: The supercell concept. *Phys. Rev. B* **2012**, *86*, 041404.

(24) Fahr, S.; Lederer, C. R. F. Engineering the randomness for enhanced absorption in solar cells. *Appl. Phys. Lett.* **2008**, *92*, 171114.

(25) Verhagen, E. Subwavelength light confinement with surface plasmon polaritons. Ph.D. thesis, Utrecht University, 2009.

(26) van de Groep, J. Light trapping in thin silicon waveguides by plasmon mediated mode coupling M.Sc. thesis, Utrecht University, 2011.

(27) van Lare, M.; Lenzmann, F.; Polman, A. Dielectric back scattering patterns for light trapping in thin-film Si solar cells. *Opt. Express* **2013**, *21*, 20738.

(28) Itoh, T.; Yamauchi, N. Surface morphology characterization of pentacene thin film and its substrate with under-layers by power spectral density using fast Fourier transform algorithms. *Appl. Surf. Sci.* **2007**, *253*, 6196−6202.

(29) Schärtl, W. *Light Scattering from Polymer Solutions and Nanoparticle Dispersions*; Springer: Heidelberg, 2007.

(30) Spinelli, P.; Verschuuren, M. A.; Polman, A. Broadband omnidirectional antireflection coating based on subwavelength surface Mie resonators. *Nat. Commun.* **2012**, *3*, 692.

(31) Ferry, V. E.; Verschuuren, M. A.; Li, H. B. T.; Verhagen, E.; Walters, R. J.; Schropp, R. E. I.; Atwater, H. A.; Polman, A. Light trapping in ultrathin plasmonic solar cells. *Opt. Express* **2010**, *18*, A237−A245.

(32) Silfvast, W. T. *Laser Fundamentals*; University of Cambridge, 2004.

(33) Mashaal, H.; Gordon, J. M. Fundamental bounds for antenna harvesting of sunlight. *Opt. Lett.* **2011**, *36*, 900−902.

(34) Nair, S. K.; Rajeev, K.; Parameswaran, K. Cloud screening in IRS-P4 OCM satellite data: potential of spatial coherence method in the absence of thermal channel information. *Remote Sens. Environ.* **2003**, *90*, 259−267.

(35) Divitt, S.; Novotny, L. Spatial coherence of sunlight and its implications for light management in photovoltaics. *Optica* **2015**, *2*, 95−103.

(36) Mersenne Twister. http://www.math.sci.hiroshima-u.ac.jp/m-mat/MT/emt.html.